

AERODYNAMIC OPTIMIZATION OF NEAR-SONIC PLANE BASED ON NEXST-1 SST MODEL

Wataru YAMAZAKI

**Department of Aeronautics & Space Engineering, Tohoku University
Aramaki-Aza-Aoba01, Aoba-Ward, Sendai, 980-8579, JAPAN**

Keywords: *Near-Sonic Plane, Aerodynamic Optimization, Unstructured Mesh, CFD*

Abstract

In this paper, aerodynamic shape optimization for an airplane cruising at the near-sonic regime is discussed based on CFD simulations. Japan Aerospace Exploration Agency (JAXA)'s experimental supersonic airplane, NEXST-1 was employed as the baseline model of the optimization. NEXST-1 was accepted as a candidate of near-sonic airplane because of the existence of 'Drag Bucket' at near-sonic regime by the past researches of the author.

In present optimization, the section airfoil shape and the planform shape were optimized independently from each other in near-sonic regime. For the optimization, Genetic Algorithm was used with unstructured mesh Euler simulations. The optimized results showed considerable improvement in L/D at near-sonic regime. The optimization of the section airfoil shape yielded to the reduction of wave drag due to shock waves. The optimization of the planform shape led to the reduction of induced drag.

1 Introduction

Recently, with the globalization of trading, human activity and transportation, the reduction of flight time between continents is demanded. In Japan, toward the realization of next generation high-speed airplanes, national experimental supersonic transport (NEXST) [1-3] was developed at the Japan Aerospace Exploration Agency (JAXA). With present technology, however, it is pointed out that supersonic transport (SST) has some difficulties such as inefficiency of fuel cost, noise pollution, air pollution, and sonic-boom. Because of such present situations, an airplane cruising at

near-sonic regime is watched with keen interest. It is considered worthy improvement in the increase of transportation efficiency and the frequent use of airplanes by about 15% improvement in the cruising speed compared with existing transonic airplanes. Moreover, the avoidance of sonic-boom because of the near-sonic cruising is an attractive advantage for airlines.

In 1970's, along with the research of supercritical airfoils, near-sonic airplanes attracted the attention and the development of a near-sonic airplane was tried at Aircraft Research Association in the U.K. [4]. At this 70's research, the near-sonic airplane was tried to be developed based on a shape as like conventional transonic airplane. Unfortunately, it was not completed at that time because of the increase of the fuel cost.

As the most famous case of a recent near-sonic airplane, Sonic-Cruiser [5] of which the Boeing Company had investigated and challenged the development is well known. The shape of Sonic-Cruiser had several new features such as canards, rear-mounted engines and two horizontal fins at the back of the airplane. The novel shape attracted researchers' and public attention. But the shape was seemed to be modified later by Boeing researchers to almost conventional one according to the September 24-30 of 2002 of 'Flight International' [6].

Considering about the aerodynamics of the near-sonic airplane, it is difficult to prevent the generation of shock wave in the near-sonic regime. So it may be effective that supersonic airplane is adopted as the baseline model of near-sonic airplane. Based on this expectation, the inspection of aerodynamics and the

preliminary design at near-sonic regime was conducted using SST model [7-8]. In these researches, JAXA's experimental SST model called NEXST-1 (Fig.1) was used. A drag minimum region, called 'Drag Bucket' was observed at the near-sonic regime by these researches. This phenomenon enhanced the possibility of NEXST-1 model as the baseline model of a near-sonic plane.

Like this way, it attracted researchers' attention what is the most suitable shape and important factor for the efficient near-sonic cruising. In this paper, therefore, aerodynamic shape optimization at the near-sonic regime based on the NEXST-1 SST model was discussed using CFD simulation. The section airfoil shape and the planform shape optimization were conducted. From the results of these optimizations, the reasons of drag reduction and the aerodynamics, especially around the shock wave, were analyzed in detail.

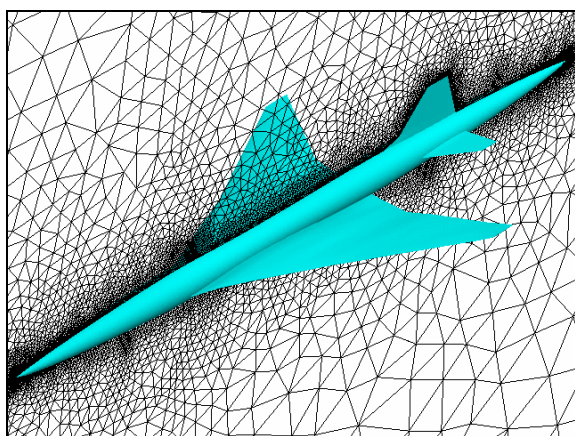


Fig.1 NEXST-1 SST Model with Unstructured Mesh

2 Computational Methods

Here, computational methods used in present optimization process were introduced.

2.1 Optimization Method

In the aerodynamic optimization, the non-linearity must be taken into consideration. So Genetic Algorithm (GA), the simulation of evolution of creatures, was adopted because it does not require the derivatives of the objective functions. In this research, GA of optimization commercial software modeFRONTIER [9] was

applied.

2.2 Aerodynamic Evaluation

In this research, a flow solver named TAS code (Tohoku University Aerodynamic Simulation), which was based on the three-dimensional unstructured mesh method was used to evaluate aerodynamic performance. In the simulation code, Euler/Navier-Stokes (NS) equations were solved by a finite-volume cell-vertex scheme. The numerical flux normal to the control volume boundary was computed using an approximate Riemann solver of Harten-Lax-van-Leer-Einfelds-Wada (HLLW) [10]. The second order spatial accuracy was realized by a linear reconstruction of the primitive gas dynamic variables inside the control volume with Venkatakrishnan's limiter [11]. The Lower/Upper Symmetric Gauss-Seidel (LU-SGS) implicit method for unstructured meshes [12] was used for the time integration.

The mesh of NEXST-1 model for the Euler computation was all tetrahedrons, and the number of nodes was about 290 thousands (Fig.1). The surface mesh was generated by advancing front method of graphical user interface (GUI) based user interactive tool, called TAS-Mesh [13]. The volume mesh was generated by Delaunay Approach [14]. For the NS computation, the hybrid volume mesh [15] composed of tetrahedrons, prisms and pyramids was used, and the number of nodes was about 1.4 millions. A one-equation turbulence model by Goldberg and Ramakrishnan was adopted to treat turbulent boundary layers [16].

By our past research [7], it was confirmed that the tendency of the aerodynamic coefficients variation was basically same between the computational results of Euler and NS at the near-sonic regime. This implied that the interference between the shock wave and the boundary layer was weak in this regime. Thus, considering about the computation cost and the required accuracy for the present optimization, Euler computation was adopted as the evaluation method of the aerodynamic performance.

3 Optimization of the Section Airfoil Shape

3.1 Optimization System

3.1.1 Geometry Definition

The optimizing modification was done regarding to the section airfoil geometry. The wing root which was 15% semi-span of wing and the wing planform shape was fixed. The design variables were totally 66. In detail, the design variables were distributed at 6 semi-span stations, 25%, 40% (kink of trailing edge), 50% (kink of leading edge), 70%, 85% and 100%. For each airfoil shape, the upper and lower surface geometries were respectively modified using 5 control points on each surface and spline curve fitting. In addition, the twist angle distribution along the span-wise direction was modified using the 6 semi-span stations as the span-wise control points. At the internal region between these stations, airfoil shape was interpolated by spline curve fitting. The outline of the geometry modification is shown in Fig.2.

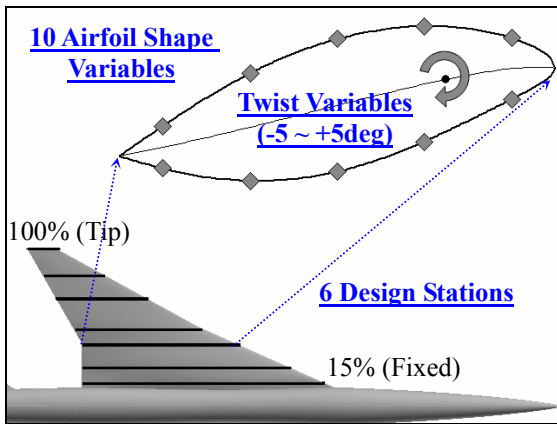


Fig.2 Design Variables Definition

3.1.2 Mesh Movement Method

These shape modification associated with the change of the design variables requires the regeneration of computational mesh. Especially, GA requires huge number of evaluations of modified airplanes. Here, this regeneration process was avoided by applying a mesh movement method based on a spring analogy [17] to NEXST-1's computational mesh. By the use of this method, the pre-process of CFD simulation of a new modified shape was done in a very short time even if the modified shape was deformed largely from the previous shape.

3.1.3 Objective & Constraints

In this shape optimization, the upper and lower curved surface including the warp plane of the main wing were optimized. The planform was fixed. The objective was to minimize pressure drag coefficient (C_{DP}) at Mach number 0.98. C_{DP} was evaluated by Euler computation. To prevent the design that has lower drag yielded to by lowering lift, the constraint that C_L kept constant (0.26) was set. This attained by adjusting the angle of attack. Moreover, to prevent the drag reduction by the design that provided a thinner wing, a constraint of keeping wing volume constant was also set.

3.2 Results & Discussion

The population size at each generation of GA was set to 30, and the probability of mutation was 0.1. All initial individuals were randomly generated. The computation has been done until 70th generation, so about 2100 times of flow simulation about differently shaped airplanes were required. The computation time was about 1 hour per 1 design by NEC SX-7 of Supercomputing System Information Synergy Center at Tohoku University. The comparison of the aerodynamic performance of NEXST-1 and the optimal design is shown in Table.1. 37 counts reduction (1count = 0.0001) of pressure drag coefficient has been achieved by the optimization. The detailed comparison between NEXST-1 and the optimal design was discussed in the following paragraphs.

3.2.1 Comparison about the Geometry

It was observed in the optimal design that the section airfoil camber increased at most of span stations. Moreover, it was also confirmed that twist angle decreased overall compared with NEXST-1.

3.2.2 Comparison about the Aerodynamics

Fig.3 is a visualization of shock function. Shock function F_{shock} is given as follows,

$$F_{shock} = (\vec{v} \cdot \nabla P) / (a \cdot |\nabla P|)$$

where \vec{v} is velocity vector, P is pressure and a represents local sonic speed. It is known that the

Table.1 Comparison of the Aerodynamic Performance of Section Airfoil Shape Optimization

	<i>Wing Volume</i>	<i>Evaluation</i>	<i>A.O.A</i>	C_L	C_{DP}	C_{Df}	L/D
<i>NEXST-1</i>	1.000	Euler	3.48 [deg]	0.26	0.01855	-	14.02
		NS	3.46[deg]	0.26	0.01965	0.01078	8.56
<i>Optimal</i>	1.003	Euler	4.02 [deg]	0.26	0.01481 -37 counts	-	17.56 +25%
		NS	4.24 [deg]	0.26	0.01596 -37 counts	0.01093	9.68 +13%

positive region of this function corresponds to compression region, and where the function is negative, it is an expansion region. Moreover, zone which $F_{shock} \geq 1$ in the compression region is upstream zone of a shock wave [18]. In Fig.3 only this upstream zone of a shock wave with entropy generation is painted. In Fig.3, two optimal results are shown. One is that of the section airfoil shape optimization which is the present subject and the other is that of the planform shape optimization which will be discussed in next chapter. It can be seen that shock wave on the outboard wing vanished and the entropy generation was reduced in the present optimal design (Section Airfoil Optimal).

Fig.4 is the comparison of C_p distributions at 40% semi-span station of the original and optimal designs. It was found that the reduction of shock strength was remarkable, and the C_p distribution was modified to rear-loading type at the optimal design. Fig.5 is shock function visualization at 40% semi-span station. Only compression regions were indicated. It was found that compression regions appeared at upstream of primary shock wave, so it was thought that gradual compression at upstream of shock wave such as isentropic compression made the reduction of shock strength.

The lift and drag forces are plotted in the span-wise direction in Fig.6. The span-wise lift variation was basically same in both of initial and optimal results. From the drag plot, it is observed that the drag decrease at outboard wing is remarkable, and this region's pressure drag force is negative. (i.e. thrust force)

Fig.7 shows C_p distribution at 85% semi-span

station, exactly thrust position mentioned just before. By the analysis, it was confirmed that the large thrust force was generated by the effect that the pressure recovery on the upper surface occurred near the wing upper crest in the optimal design. That is to say, this phenomenon to cause thrust force on the outboard wing was done by the optimized position of the pressure recovery on the upper wing.

3.2.3 Validation Study of Present Optimization

Fig.8 is the comparison of C_{DP} -Mach curves of NEXST-1 which was the original design and the optimal design at $C_L=0.26$. In Fig.8, two optimal results are plotted in the same way with Fig.3. The drag minimum region appeared in the near-sonic regime was called 'Drag Bucket' as mentioned before. From the figure, the good off-design performance of the optimal design (Blue line titled by *Section Airfoil*) was confirmed. At the whole range of transonic and near-sonic regime, from 15 to 30% improvement was achieved. Moreover, off-design performance as concerns the angle of attack, mesh dependency effect and viscous effect (i.e. NS computation) were also analyzed. These results showed good performance on the whole. The NS computation results were also included in Table.1. It was confirmed that the NS computation results showed same level drag reduction of C_{DP} with Euler Computation.

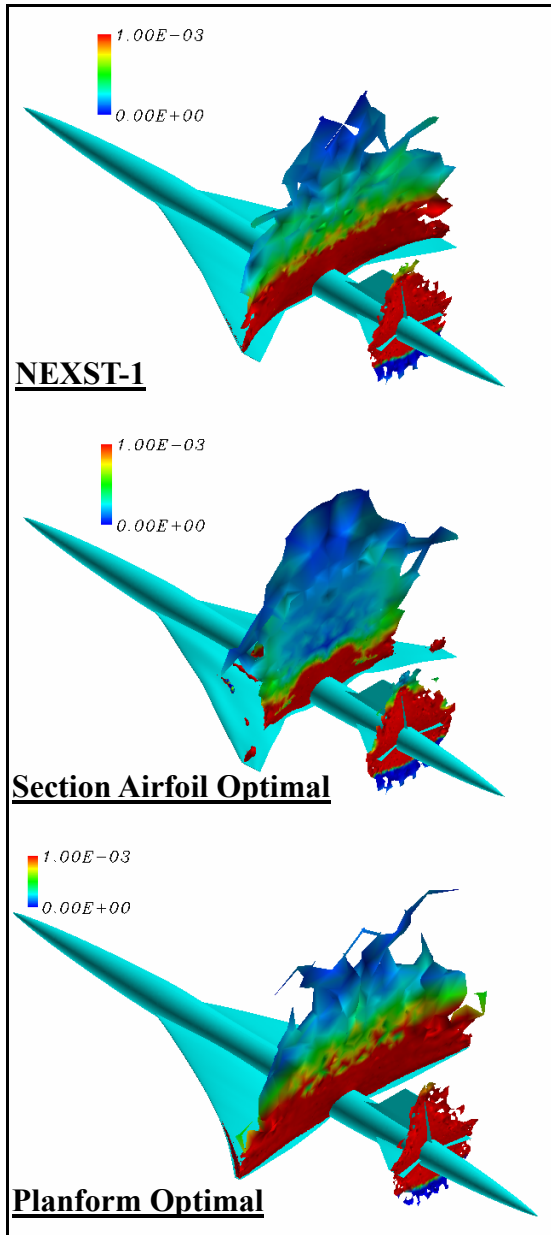


Fig.3 Shock & Entropy Visualization

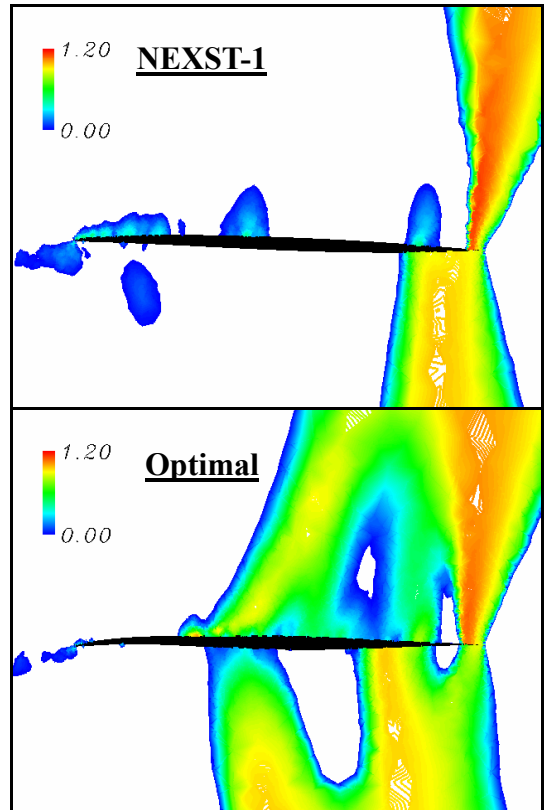


Fig.5 Shock Function Visualization at 40% Semi-span

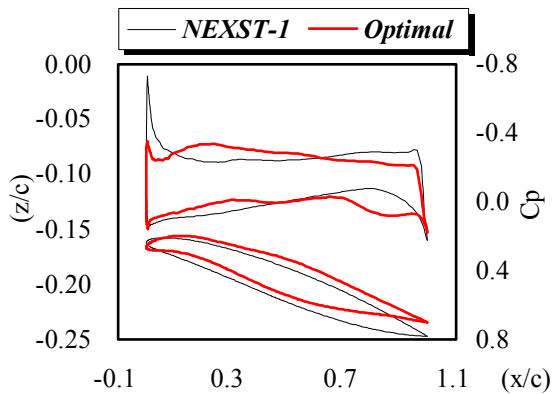


Fig.4 Cp Distribution at 40% Semi-span

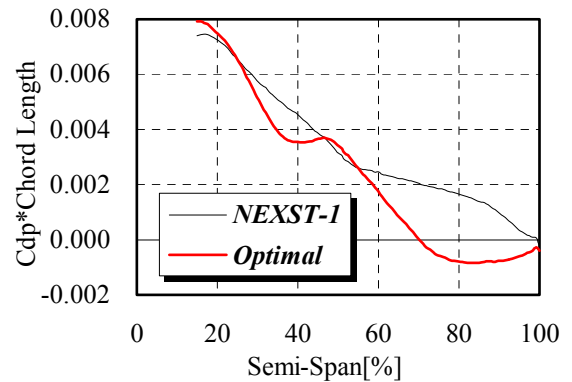
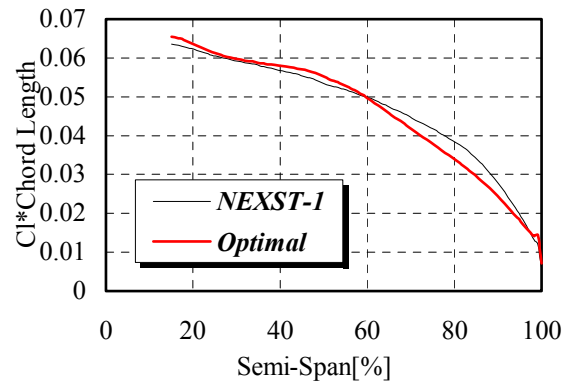


Fig.6 Lift & Pressure Drag Distribution Plot in the Span-wise Direction

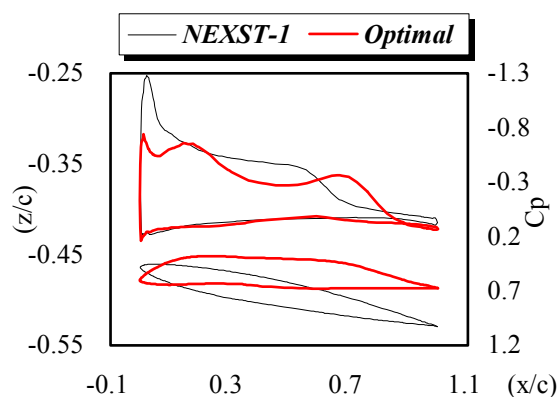
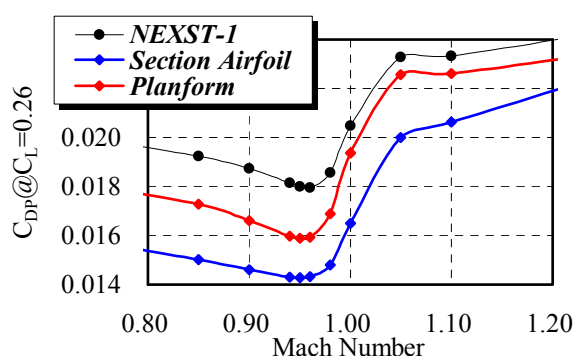


Fig.7 Cp Distribution at 85% Semi-span

Fig.8 Drag Bucket @ $C_L=0.26$

4 Optimization of the Planform Shape

Section airfoil shape optimization conducted in the previous chapter showed good improvement in the L/D. But the optimized value of L/D was still poor for the efficient cruising in near-sonic regime and further optimization in a larger design space were required. In this chapter, therefore, aerodynamic optimization of the planform shape was conducted as one of the further optimization.

4.1 Optimization System

4.1.1 Geometry Definition

The optimization of the wing planform shape was conducted in this chapter. For the fuselage and tail wing of a new airplane, the shape of those of the NEXST-1 SST model was used as they had been. The wing-fuselage junction geometry was also fixed for the simplicity of the generation of computational mesh (it will be

mentioned later) and the reduction of design variables. The outline of the parametric definition of the planform shape based on the design variables was shown in Fig.9. The planform's basic shape was defined by 5 design variables; x and y coordinates of the wing kink (X_{kink} , Y_{kink}), the chord length at the kink (C_{kink}), and x and y coordinates of the wing tip (X_{tip} , Y_{tip}). The chord length at the wing tip was calculated automatically according to the given condition that the reference wing-area (S_{ref}) constant. Moreover, the leading edge line was determined by 3 control points (root, kink and tip of leading edge) by the linear (Double-Delta Wing) or spline curve (Ogee Wing) interpolation. It was switched by another 1 design variable ($DorO$).

The section airfoil shape was decided by following rule; a section airfoil shape was interpolated by that of NEXST-1 model of corresponding semi-span length. It contributed to the reduction of design variables relating to the section airfoil shape. This definition of the section airfoil shape also made the non-dimensional thickness of airfoil (t/c) at every span station constant during optimization, which contributed to the elimination of some constraints relating to the section airfoil thickness. Initially, the twist angle distribution of new modified airplane was set to be same with that of NEXST-1. Then the twist angle distribution was modified using spline curve technique by 4 design variables (TW) which distributed at 40%, 60%, 80% and 100% semi-span stations respectively. Therefore, the number of design variables was 10 totally. The acceptable range of these design variables was described in Table.2.

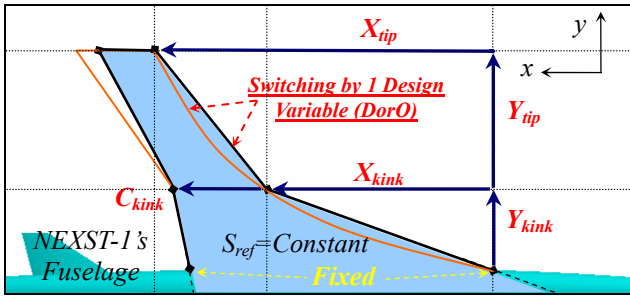


Fig.9 Wing Planform Shape Definition

Table.2 Acceptable Range of Design Variables

Fuselage Length	$L = 1.0$ (Unit Length)
Chord Length @Root	$C_{root} \sim 0.333$ (Fixed)
Reference Wing Area	$S_{ref} = 0.03826$ (Fixed)
Inboard Span Length	$0.02 < Y_{kink} < 0.15$
Outboard Span Length	$0.02 < Y_{tip} < 0.15$
Chord Length @Kink	$0.05 < C_{kink} < 0.25$
X-Coordinate @Kink	$0 < X_{kink} < 0.457$
X-Coordinate @Tip	$0 < X_{tip} < 0.457$
Modification Range of Twist Angle	$-5deg < TW < +5deg$

4.1.2 Regeneration of Computational Mesh

The mesh movement method worked well for the wing section shape design shown in previous chapter. However, it could not handle the planform shape modification which required larger modification of computational mesh. For the construction of automatic optimization system of the planform design, generation processes of the wing surface mesh and the volume mesh have to be done automatically. In this research, it was achieved by the following strategies which were the new combination of existing tools.

1) Geometry Definition;

It was explained in previous section (4.1.1).

2) Definition of Mesh Point Distribution at Surface Patch's Boundaries;

Wing's surfaces on which the surface mesh should be generated are divided into 3 patches in this research; they are a wing upper, a wing lower and a wing tip patched surfaces. Suitable mesh point distribution is given at boundaries of these patches. Boundaries are composed of the leading edge, the trailing edge and the wing tip. At the wing-fuselage junction boundaries, the mesh point distributions are set to agree with

that of NEXST-1's fuselage surface mesh which already generated by TAS-Mesh.

3) Surface Mesh Generation;

Surface meshes of wing upper, lower and tip are generated based on Delaunay triangulation algorithm. At first, surface boundary's mesh points given in 2) are interpolated (Fig.10.a & .b). Next, for the maintenance of the solution accuracy and the sufficiently accurate geometrical expression, the inner nodes are interpolated densely around the leading edge (Fig.10.c). After that, other inner nodes are generated and then interpolated based on Weatherill's method (Fig.10.d).

4) Fusion of Surface Meshes;

Surface meshes on the wing upper, lower and tip planes generated by 1), 2), 3) process and the surface meshes of the fuselage and tail wing of NEXST-1 already generated are united into one surface mesh (Fig.10.e).

5) Volume Mesh Generation;

Volume mesh generation is done automatically using Delaunay tetrahedral meshing approach (Fig.10.f) [14]. The number of nodes is adjusted to almost 300,000 points which is the best balanced number for the computational accuracy and the cost.

By the use of this system, the pre-process of CFD simulation of a new modified airplane was done robustly in acceptable computation time. In Fig.11, several examples of randomly generated geometries based on this system with the pressure distribution at Mach number 0.98 were shown.

4.1.3 Objective & Constraints

The objective was to minimize pressure drag coefficient (C_{DP}) which was computed by the Euler code at cruising Mach number 0.98. The constraints that C_L kept constant (0.26) was realized by adjusting the angle of attack. Another constraint that the wing inside volume of the designed airplane should be greater than that of NEXST-1 was also set.

Table.3 Comparison of the Aerodynamic Performance of Planform Shape Optimization

	<i>Wing Volume</i>	<i>Aspect Ratio</i>	<i>Evaluation</i>	<i>A.O.A</i>	C_L	C_{DP}	$L/D_{inviscid}$
<i>NEXST-1</i>	1.000	2.20	Euler	3.48 [deg]	0.26	0.01855	14.02
<i>Optimal</i>	1.047	2.48 +13%	Euler	3.29 [deg]	0.26	0.01689 -17counts	15.40 +9.8%

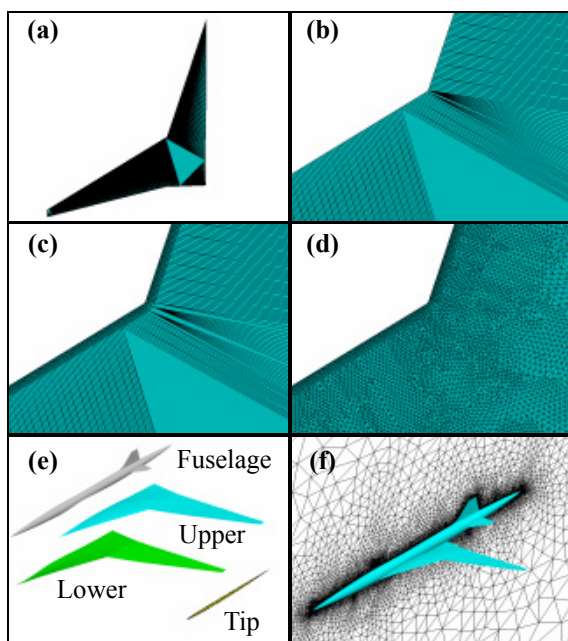


Fig.10 Automatic Mesh Generation Procedures;

- (a) Interpolation of Surface Boundary's Mesh Points,
 (b) Zoomed View around the Kink of Leading Edge,
 (c) Inner Node Interpolation around the Leading Edge,
 (d) Inner Node Interpolation by Weatherill's Method,
 (e) Fusion of Generated Surface Meshes,
 (f) Volume Mesh Generation around the Airplane

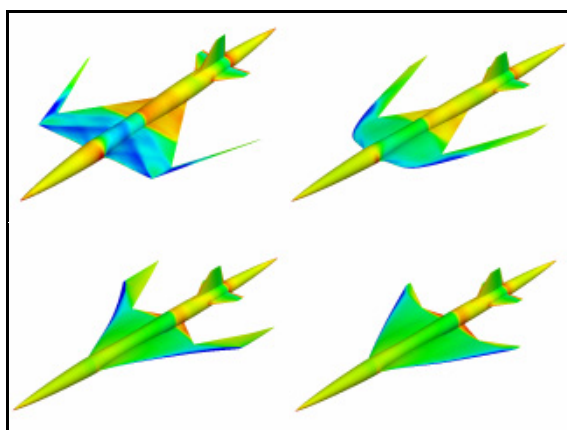


Fig.11 Several Computation Examples of Randomly Generated Airplanes

4.2 Results & Discussion

In the optimization, GA was used. The population size at each generation was set to 20, the probability of mutation was 0.1, and all initial individuals were randomly generated. The computation has been done until 30th generation, so 600 times of the flow simulation about differently shaped airplanes were required. The unstructured mesh generation and the aerodynamic evaluation of 1 individual demanded about 2 hours for the computation using NEC SX-7. The aerodynamic performance of NEXST-1 and the optimal design was compared in Table.3. Keeping the wing inner volume and C_L constant, 17counts reduction of C_{DP} was achieved. The comparison between NEXST-1 and the optimal design was discussed in the following section.

4.2.1 Comparison about the Geometry

The planform shape of the optimal design was shown in Fig.12 with that of NEXST-1. It was observed that 13% increase of the aspect ratio and the modification of the wing planform shape from Double-Delta to as like Delta wing. Moreover, it was confirmed that the twist angle distribution was almost same with that of NEXST-1 which had been optimized for the supersonic cruising of Mach 2.0.

4.2.2 Comparison about the Aerodynamics

The lift and pressure drag distribution in the span-wise direction was shown in Fig.13. The span-wise lift distribution was modified to more elliptical one than that of NEXST-1. The span-wise pressure drag distribution was almost same with that of NEXST-1.

Fig.14 is the comparison of C_p distribution at 40% semi-span station. The visualization of the shock location with entropy generation was

included in Fig.3 (Planform Optimal). It was understood that the shock location was almost same with that of NEXST-1 and the shock strength was almost same with that of NEXST-1. The induced drag reduction based on the increase of the aspect ratio was estimated about 14counts by the lifting line theory (Oswald efficiency factor was assumed 0.80). This drag reduction level was agreed with that achieved by present planform optimization. Therefore, it was concluded that the induced drag was mainly decreased in present optimization while the wave drag was kept almost constant.

The C_{DP} -Mach curves of the optimal design (Red line titled by *Planform*) at $C_L=0.26$ was included in Fig.8. Although the optimized performance achieved in this chapter was inferior to that achieved in previous chapter (Blue line titled by *Section Airfoil*), the good off-design performance of the optimal design was confirmed. It was thought that the reason why excellent improvement was not achieved by present planform optimization was because of the strong constraint such as the S_{ref} , wing inner volume and (t/c) constant as well as the fixed wing root length.

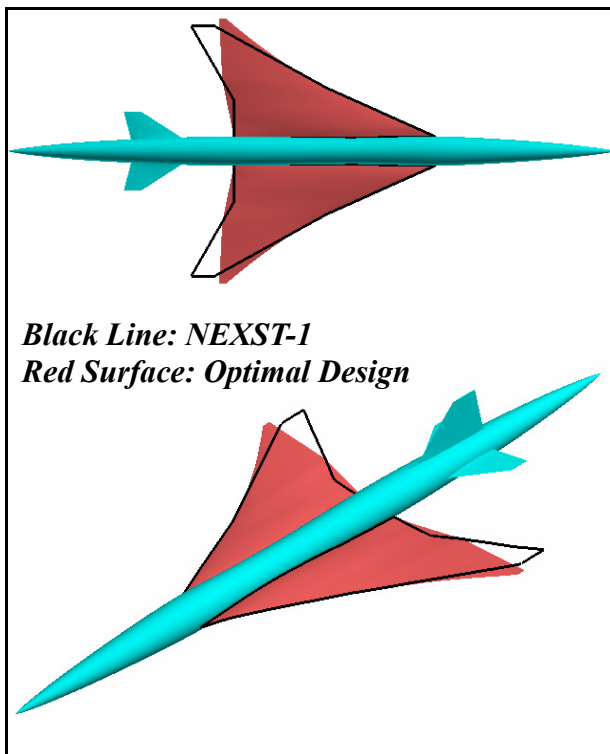


Fig.12 Geometry of the Optimal Airplane

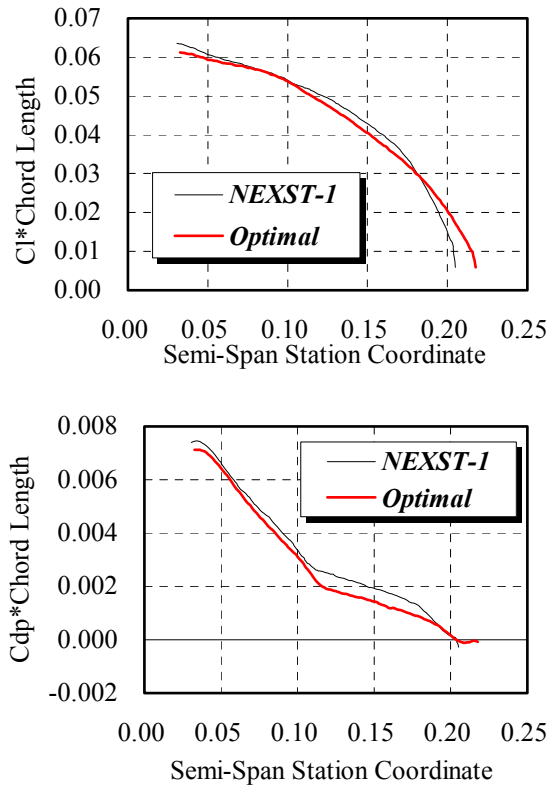


Fig.13 Lift & Pressure Drag Distribution Plot in the Span-wise Direction

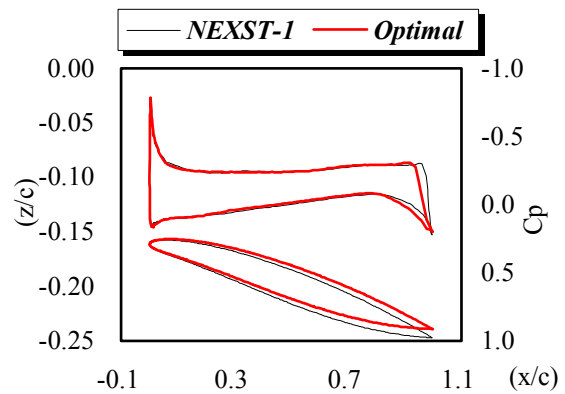


Fig.14 Cp Distribution at 40% Semi-span

5 Conclusions

In this paper, two aerodynamic optimizations of near-sonic plane were conducted using Genetic Algorithm with unstructured mesh flow simulation method. One was the section airfoil shape optimization and the other was planform shape optimization. For both optimizations, NEXST-1 SST model was used as the baseline model. To enhance the efficiency and the robustness of the optimization, the mesh

movement method and the automatic unstructured mesh generation system was applied in the optimization.

By the optimization of NEXST-1 SST model's section airfoil shape, significant C_{DP} reduction was achieved. It was confirmed that the wave drag was mainly reduced in this optimization. A wing surface geometry which caused isentropic compression at upstream of shock wave was important factor for the C_{DP} reduction in near-sonic regime. Moreover, the optimized position of the pressure recovery on the outboard wing realized thrust pressure force at the optimal design.

Another C_{DP} reduction was achieved by the planform optimization. In this optimization, the induced drag was mainly decreased while the wave drag was kept almost constant. The reduction of C_{DP} by the planform optimization was not satisfactory big. This is because the given constraints were too much to allow the flexible shape change.

In the present study, the important mechanisms to improve the L/D of a near-sonic airplane were clarified. Therefore, with the full shape optimization of the wing section, planform and fuselage, it will be feasible to realize an efficient near-sonic airplane whose L/D is similar to the conventional transonic transport.

Reference

- [1] Sakata, K.: Supersonic Experimental Airplane (NEXST) for Next Generation SST Technology, AIAA Paper 2002-0527, 2002.
- [2] Matsushima, K., Iwamiya, T. and Ishikawa, H.: Supersonic Inverse Design of Wings for the Full Configuration of Japanese SST, Proceedings of the 22nd ICAS Congress, pp.213.1-213.8, 2000.
- [3] Matsushima, K., Iwamiya, T. and Nakahashi, K.: Wing Design for Supersonic Transports Using Integral Equation Method, *Engineering Analysis with Boundary Elements* 28, pp.247-255, 2004.
- [4] Haines, B.: The Aerodynamic Design of the Wing-Fuselage for a Near-Sonic Transport, AIAA Paper 2002-0517, 2002.
- [5] Boeing Company web page:<http://www.boeing.com>
- [6] Flight International web page:<http://www.flightinternational.com>
- [7] Matsushima, K., Yamazaki, W. and Nakahashi, K.: Transonic Design of SST, Proceedings of IUTAM Symposium TRANSSONICUM IV, Germany, 2002.
- [8] Takenaka, K., Nakao, M., Yamamoto, K. and Takaki, R.: Flow analysis and its validation of NEXST-1 near Mach 1, 16th CFD symposium C13-4, Japan, 2002 (in Japanese).
- [9] ESTECO s.r.l. web page: <http://www.esteco.it>
- [10] Obayashi, S. and Guruswamy, G. P.: Convergence Acceleration of a Navier-Stokes Solver for Efficient Static Aeroelastic Computations, *AIAA Journal*, Vol.33, No.6, pp.1134-1141, 1995.
- [11] Venkatakrishnan, V.: On the Accuracy of Limiters and Convergence to Steady State Solutions, AIAA Paper 93-0880, 1993.
- [12] Sharov, D. and Nakahashi, K.: Reordering of Hybrid Unstructured Grids for Lower-Upper Symmetric Gauss-Seidel Computations, *AIAA Journal*, Vol.36, No.3, pp.484-486, 1998.
- [13] Ito, Y. and Nakahashi, K.: Surface Triangulation for Polygonal Models Based on CAD Data, *International Journal for Numerical Methods in Fluids*, Vol.39, Issue 1, pp.75-96, 2002.
- [14] Sharov, D. and Nakahashi, K.: Hybrid Prismatic/Tetrahedral Grid Generation for Viscous Flow Applications, *AIAA Journal*, Vol.36, No.2, pp.157-162, 1998.
- [15] Ito, Y. and Nakahashi, K.: Unstructured Mesh Generation for Viscous Flow Computations, Proceedings of the 11th International Meshing Roundtable, Ithaca, NY, pp.367-377, 2002.
- [16] Goldberg, U. C. and Ramakrishnan, S. V.: A Pointwise Version of Baldwin-Barth Turbulence Model, *Computational Fluid Dynamics*, Vol.1, pp.321-338, 1993.
- [17] Murayama, M., Nakahashi, K., and Matsushima, K.: Unstructured Dynamic Mesh for Large Movement and Deformation, AIAA Paper 2002-0122, 2002.
- [18] Papparone L. and Tognaccini R.: Computational Fluid Dynamics-Based Drag Prediction and Decomposition, *AIAA Journal*, Vol.41, No.9, pp.1647-1657, 2003.